Li, Q., Zhu, Y. Q., & Eichhorn, S. J. (2019). Carbonized Electrospun Cellulose Composite Nanofibres Containing Silicon Carbide Nanoparticles. *Composites Part A: Applied Science and Manufacturing*, *123*, 71-78. https://doi.org/10.1016/j.compositesa.2019.04.028

Carbonized Electrospun Cellulose Composite Nanofibres Containing Silicon Carbide Nanoparticles

Qiang Li[1], Yanqiu Zhu[1], Stephen J. Eichhorn[2*]

1. College of Engineering, Maths & Physical Sciences, North Park Road, University of Exeter, Exeter, Devon, EX4 4QF, UK
2. Bristol Composites Institute (ACCIS), School of Civil, Aerospace and Mechanical Engineering, University Walk, University of Bristol, Bristol, BS8 1TR, UK.

Abstract

Carbon nanofibres (CNF)/silicon carbide (SiC) composites have been fabricated by electrospinning of cellulose acetate and SiC nanoparticles, followed by deacetylation and carbonization. Carbon nanotubes (CNTs) were then grown on the surface of the CNF/SiC composite nanofibres via a chemical vapor deposition (CVD) method. Raman spectroscopy was used to characterize the crystallinity of CNF/SiC and CNF/SiC/CNTs samples by comparing the Raman D and G band intensity ratio (I_D/I_G), and the full width at half maximum (FWHM) of bands. Elastic modulus of the CNF/SiC/CNTs fibres was estimated using a Raman spectroscopic method by observing the shift of the 2D Raman band during tensile deformation of the fibre composites; a value of 166 ± 28 GPa was estimated, which is comparable to medium stiffness commercial carbon fibre filaments. The unique structure of these composite nanofibres combined with their high modulus could make them useful as reinforcements for composite materials.

* Corresponding author. Tel./fax/: +44 (0)44 117 33 15650
E-mail address: s.j.eichhorn@bristol.ac.uk (S. J. Eichhorn)

1 Introduction

Carbon fibres (CFs) are useful for reinforcing composite materials because they have high specific modulus and high specific strength [1]. The mechanical properties of CF composites could benefit from forming a more complexed structure [2]. To achieve this in the past, ceramic nanoparticles have been added into CF composites to achieve an improvement in the mechanical properties [3].

Silicon carbide (SiC), a widely used ceramic material, exhibits excellent properties such as high abrasive resistance, low thermal expansion, superior chemical compatibility, good thermal conductivity, high strength, modulus and low density [4]. Because of these outstanding properties, SiC nanoparticles have the potential to act as a reinforcing material for CF composites [5]. Several methods have been demonstrated for the fabrication of CF/SiC composites; *e.g.* by coating SiC on the fibre's surface [6], and conventional chemical vapor infiltration methods [7]. The production of CF/SiC composites however has issues with weak interactions between the CF and the SiC nanoparticles and agglomeration of the latter [8, 9]. To address these issues, one effective strategy is to *in-situ* synthesize the CF/SiC composites. During this process, the formation of strong interactions between the CF and SiC nanoparticles prevents the nanoparticles from agglomerating and/or detaching from the surface [9]. Electrospinning is one of the best approaches to achieve the *in-situ* synthesis of CF/nanoparticle composites [10]. Specifically, CF/SiC composites can be produced by using an electrospun solution that contains both SiC nanoparticles and a CF precursor. Cellulose, as a renewable precursor for CF, has been previously regenerated from electrospun cellulose acetate (CA) nanofibres *via* deacetylation [11]. This approach overcomes some of the issues that occur when spinning directly from cellulose, such as poor solvation and an inability to volatilise the solvent. Furthermore, the growth of CNTs on the surface of CF/SiC composites by a chemical vapor

deposition (CVD) is thought to enhance their mechanical properties. Improved mechanical properties have been previously demonstrated by growing CNTs on CF substrates [12].

Herein we describe the production of electrospun carbon nanofibres (CNF) with incorporated SiC nanoparticles. CNTs were subsequently grown on the surface of the CNF/SiC nanofibres by the CVD technique. The elastic modulus of the CNF/SiC/CNTs composite nanofibres was estimated using an *in-situ* Raman spectroscopic method. This approach demonstrates that medium modulus (~200 GPa) carbon nanofibres can be produced, which could find applications in composite materials.

2 Experimental methods

2.1 Materials

Cellulose acetate (average M_n = 100,000 g mol^{-1}) was dissolved in a mixed solution of acetone and N,N-dimethylacetamide (DMAc) (2:1 w/w). Following this, SiC nanoparticles with a particle size < 100 nm (Sigma-Aldrich, Dorset, UK) were added to the mixed solution of CA/DMAc/acetone. The concentrations of CA and SiC were 20 and 0.4 wt.%, respectively. The CA/DMAc/acetone/SiC solution was stirred using a magnetic stirrer overnight at room temperature.

2.2 Electrospinning of composite nanofibres

Electrospinning was carried out using the mixed CA/DMAc/acetone/SiC suspension. The electrospinning set-up consisted of a syringe connected to a pump (Harvard apparatus, Holliston, USA), a voltage supplier (Electrospinz, Blenheim, New Zealand), an Al foil collector (Fisher-Scientific, Loughborough, UK), and a platform (Electrospinz, Blenheim, New Zealand). Optimal spinning conditions were found; namely a voltage of 20 kV, a flow rate of 1

mL h^{-1} and a needle tip-to-collector distance of ~13 cm. Electrospun CA/SiC fibres were spun onto an Al foil collector over a period of 3 h. The as-spun CA/SiC fibrous mats were then deacetylated in a 0.05 M NaOH/ethanol solution for 48 h to allow them to regenerate into cellulose/SiC fibres. The fibrous mats were then rinsed with water until neutral and then dried in air.

2.3 Carbonization of the cellulose fibres

Regenerated cellulose/SiC fibres were firstly stabilized by heating to 240 °C from room temperature in air at a rate of 5 °C min^{-1}, followed by keeping at a stable maximum temperature for 60 min. These stabilized fibres were then carbonized by heating to 900 °C in an Ar atmosphere at a heating rate of 10 °C min^{-1}, followed by keeping at the final maximum temperature (900 °C) for 30 min. The carbonized regenerated cellulose fibres containing SiC are denoted as CNF/SiC.

2.4 CVD production of CNTs

The CNF/SiC sample was pre-located in the hot zone of a CVD furnace. This furnace was then heated to 800 °C at a heating rate of 10 °C min^{-1}. A mixture of ferrocene/styrene (0.01 g ml^{-1}) was fed into the CVD furnace at a flow rate of 1.3 cm^3 h^{-1} for 25 min. The CNF/SiC fibres after CVD treatment are denoted as CNF/SiC/CNTs.

2.5 Characterisation of samples using Electron Microscopy and X-ray Diffraction

A Scanning Electron Microscope (SEM) (HITACHI S3200N SEM-EDS) with a voltage of 20 kV was utilized to observe the morphologies of the CA/SiC, regenerated cellulose/SiC, CNF/SiC, and CNF/SiC/CNTs fibre samples. A Transmission Electron Microscope (TEM) (JEOL 2100) was used to examine the nanostructures and the morphologies of the CA/SiC and

CNF/SiC fibres. To prepare the TEM samples, the CA/SiC fibres were directly collected onto a copper grid during electrospinning, while the CNF/SiC fibres were sonicated in ethanol for 15 min and deposited onto the grids. Selective Area Electron Diffraction (SAED) within the TEM was used to identify the polytypes of the SiC nanoparticles.

2.6 Characterization of the composite nanofibres using Raman spectroscopy

A Renishaw RM1000 Raman spectrometer with a laser of wavelength of 532 nm was utilized to record spectra from the SiC nanoparticles, CA, CA/SiC, regenerated cellulose, regenerated cellulose/SiC, CNF/SiC, and CNF/SiC/CNTs fibres. It was also used to record the spectra for the *in-situ* Raman spectroscopy/bending experiments on the CNF, CNF/SiC, and CNF/SiC/CNTs samples. A Leica CCD detector was used to record the spectral output. The laser spot size was ~1 - 2 μm, and the power was ~1 mW when the laser was focused on the sample using a 50× objective microscope lens. For each measurement an exposure time of 30 s was used.

For *in-situ* Raman spectroscopy studies, a 5 mm × 5 mm square sample of the CNF, CNF/SiC, or CNF/SiC/CNT fibre mats was placed centrally on a 70 mm × 22 mm × 1.5 mm poly(methyl methacrylate) (PMMA) beam. Two drops (0.25 mL) of a 0.1 g ml^{-1} PMMA/acetone mixed solution were deposited on the top of these samples and dried at room temperature for 1 h. A strain gauge (type CEA-06-240UZ-120, Vishay Micro-Measurements) was attached to the surface of the PMMA beam using cyanoacrylate adhesive. Two wires were soldered to each copper tab of the strain gauge, which was connected to a transducer. A four-point bending rig was used to deform the samples in tension. Raman spectra were recorded in 0.05 % strain increments up to 0.6 % strain. Figure 1 shows a schematic of the *in-situ* Raman and deformation studies.

3 Results and discussion

3.1 SEM characterization of composite nanofibres

Typical SEM images for the as-spun CA/SiC fibres and regenerated cellulose/SiC fibres are shown in Figures 2a and 2b. The regenerated cellulose/SiC fibres are not as straight as the CA/SiC fibres, possibly as a result of the regeneration process. SEM images were also obtained for the CNF/SiC fibres; typical examples are shown in Figures 2c and 2d. The average diameter of the CNF/SiC fibres was found to be 491 ± 290 nm. Some clusters of SiC nanoparticles are clearly present on the surfaces of the CNF fibres. These clusters are thought to form because the SiC nanoparticles protrude from the surface of the CNFs when the diameter of the regenerated cellulose fibres reduces due to shrinkage during the carbonization process. Aggregation of SiC nanoparticles inside the CNFs is due to the small diameter of the fibres which increases the possibility of formation of SiC clusters. Aggregation of nanoparticles is well known, and typically occurs due to their high surface to volume ratios and thereby increased van der Waal interactions. Typical SEM images of CF900/SiC/CNTs fibres are shown in Figures 2e and 2f, showing that the CNTs completely cover the surface of the fibres. The areal density of the CNTs on the CNF/SiC fibres is measured to be 4.5 mg cm^{-2}. This demonstrates that an increased flow rate of styrene/ferrocene (from 0.8 to 1.3 cm^3 h^{-1}) leads to an improved CNT yield; this is an increase of CNT production compared with a previous study [11].

3.2 TEM characterization of composite nanofibres

Typical TEM images of the composite nanofibres are shown in Figure 3. Figures 3a and 3b show that there are more SiC nanoparticle clusters present on the surface of the CNF samples compared to the as-spun CA fibres. In Figure 3c, the lines presented in the inset are closely

related to planes of atoms in the crystalline lattice of SiC. The *d*-spacing of the marked planes is estimated from these lines to be ~0.25 nm; this value corresponds to the *d*-spacing of the (111) planes [13]. Crystal defects such as stacking faults can be seen (black lines within the marked dashed rectangle in Figure 3c); in some particles many stacking faults are observed (Figure 3d). The presence of stacking faults for the 3C-SiC polytype has been reported in a previous study [14]. SAED was carried out using the TEM electron beam to confirm the polytypes of the SiC nanoparticles. Diffraction patterns were obtained by focusing on a single SiC particle in Figure 3c. Miller indices of the spots, observed in the diffraction patterns from SAED of the SiC particles, are found to be (111), (220) and (222); these correspond to *d*-spacings of 0.25, 0.15 and 0.12 nm, respectively as shown in Figure 3e. These three planes correspond to the planes of the 3C-SiC polytype [15].

3.3 Raman spectroscopic characterization of SiC composites

Typical Raman spectra for SiC nanoparticles, CA, CA/SiC, regenerated cellulose and regenerated cellulose/SiC composite nanofibres are shown in Figure 4a. The Raman bands located at ~ 656 and 1739 cm^{-1} are observed for CA and CA/SiC but are absent for the regenerated cellulose and regenerated cellulose/SiC samples. Specifically, the band located at ~ 656 cm^{-1} corresponds to stretching mode vibrations of C=O bonds emanating from ester groups [16]. The other band located at ~ 1739 cm^{-1} corresponds to the vibration of the carbonyl bonds (C=O) present in the acetyl groups [17]. In addition, the band located at ~ 796 cm^{-1} for the SiC, CA/SiC and regenerated cellulose/SiC samples corresponds to the zone center transverse optical phonon (TO) mode for the 3C-SiC polytype (β-SiC) [18]. In addition, an intense peak is located at ~1095 cm^{-1} in the regenerated cellulose and regenerated cellulose/SiC samples, which is attributed to the C-O ring and glycosidic linkage stretching modes, indicating the presence of cellulose [19]. Samples that contain SiC exhibit bands located at ~1352 cm^{-1}

and ~1600 cm^{-1}, which are respectively assigned to D and G bands of the graphite layers of carbon deposits, in agreement with the findings of other studies [20, 21]. These bands may arise due to the production of carbon deposits in the SiC particles during manufacturing.

Typical Raman spectra for the carbon CNF/SiC and CNF/SiC/CNTs samples are shown in Figure 4b. Both exhibit characteristic Raman bands located at ~1350 cm^{-1} (D band) and ~1590 cm^{-1} (G band). The Raman band observed at ~796 cm^{-1} for the CNF/SiC sample corresponds to the TO mode in the 3C-SiC polytype. This band is however absent after the growth of CNTs, which is thought to be due to the full coverage of CNTs on the CNF/SiC surface, which hinders the interaction between the spectrometer laser and the SiC. There is a low intensity Raman band located at ~2682 cm^{-1} that is observed for the CNF/SiC/CNTs sample. This band is called 2D band, which is caused by an overtone of the D band and is normally present in Raman spectra from multi-walled CNTs [22].

The intensity ratio for the D and G bands (I_D/I_G) has been used to quantify disorder in carbon materials [23]. The magnitude of the I_D/I_G ratio is thought to be representative of a lateral crystal size $L_a < 2$ nm for the CNF/SiC samples [24]. The relationship between the I_D/I_G ratio and L_a, therefore, obtained for $L_a < 2$ nm is [11, 25, 26]

$$I_D/I_G = 0.0062\, L_a^2 \qquad (1)$$

For a crystallite size larger than 2 nm, with a Raman laser wavelength $\lambda = 532$ nm, the evolution of disorder is typically quantified using the Tuinstra–Koenig relationship [27], described by the equation

$$I_D/I_G = 49.5\,\text{Å}/L_a \quad (2)$$

The intensity ratio for the D and G bands (I_D/I_G) increases after the growth of CNTs; from 1.19 ± 0.02 to 1.31 ± 0.02 (Table 1), indicating a larger value of L_a for this sample. In theory, a CF with a larger L_a indicates an increase in the degree of graphitization, and an increased grain size, which results in stronger sp^2 carbon bonds and in turn improved mechanical properties and electrical resistivity [28]. The increased I_D/I_G ratio also indicates that there are more defects in the CNF/SiC/CNTs sample; an increase in defects has been shown to increase the mechanical strength of graphitic structures due to an increased anisotropy between the in-plane and out-of-plane directions [28].

The full width at half maximum (FWHM) of the D and G bands is another indicator of crystallinity in carbonaceous materials. The FWHM of both D and G bands tends to decrease after the growth of CNTs (Table 1). The FWHM of the D and G bands in CNF/SiC sharply decreases from 250.8 ± 3.0 to 149.1 ± 1.3 cm^{-1} and 99.4 ± 2.0 to 69.3 ± 1.1 cm^{-1}, respectively. This decrease is thought to occur because of the presence of the well-ordered carbon structure of the CNTs [29].

Shifts in the position of the G band upon tensile deformation have been previously used to investigate the stress-transfer behaviour between resins and carbon fibres [30]. In our study, however, no obvious G band shifts were observed for CNF, CNF/SiC, and CNF/SiC/CNTs (Figure 5a-c). This lack of a clear shift is possibly because the ordered carbon structures for CNF and CNF/SiC are not well developed below a carbonization temperature of 900 °C. In addition, for the samples with CNTs grown on the surface, the G band is not sensitive to strain. This is surprising since the CNTs are highly crystalline, but some averaging between the poorly

formed carbon fibres and these structures might occur. The position of the 2D Raman band is however thought to be extremely sensitive to tensile deformation [31]; this band is then used to study the stress transfer properties between the resin and CNF/SiC/CNTs. Figure 6a shows that tensile deformation of these samples causes an apparent downshift in the position of the 2D band in the range from 0 to 0.6 % strain; the 2D band shift has an approximately linear relationship with the level of applied deformation. We excluded two data points from the fit to these shifts as they were positive (>0), which would normally indicate compression of the structure. Using the slope of a linear regression of the data, the strain dependence of the Raman band shift, $(\mathrm{d}(\Delta\nu)/\mathrm{d}\varepsilon)$, for the 2D band, is found to be -8.3 cm^{-1} $\%^{-1}$. The Young's modulus of the fibres can be related, in the elastic limit, to the Raman band shifts with respect to both stress and strain using the equation

$$E = \frac{\mathrm{d}\sigma}{\mathrm{d}(\Delta\nu)} \times \frac{\mathrm{d}(\Delta\nu)}{\mathrm{d}\varepsilon} = \frac{\mathrm{d}\sigma}{\mathrm{d}\varepsilon} \qquad (3)$$

where E is the Young's modulus and $\mathrm{d}(\Delta\nu)/\mathrm{d}\varepsilon$ is the rate of Raman band shift with respect to strain. The stress sensitivity of the Raman band shift is expressed by $(\mathrm{d}(\Delta\nu)/\mathrm{d}\sigma)$, where $\Delta\nu$ is the value of Raman band shift and σ is the stress. The value of stress sensitivity of the Raman 2D band shift has been reported to be -5 cm^{-1}/GPa for CNT [32]. Using equation 3, and this value of stress sensitivity, we estimate an elastic modulus (E) of 166 ± 28 GPa for the CNF/SiC/CNTs sample. This value is slightly smaller than commercial T650 and IM-7 CFs (200 GPa; [33]), indicating that the CNF/SiC/CNTs composite fibres have high stiffnesses. The modulus of the CNF/SiC/CNTs fibres is also higher than that for the plain CNFs produced at 1500 °C (60 GPa) and 2200 °C (100 GPa), that were obtained using similar methodology [19]. The modulus of the composite CNF/SiC/CNTs nanofibres is however much lower than pure individual multi-walled CNTs (1.7 – 2.4 TPa) [34], which may be due to the presence of the

less crystalline CNF fibres.

Figure 6b shows a plot of I_D/I_G versus L_a for the CNF/SiC/CNTs, together with the data from previously published work [19, 24, 35]. The relationship between L_a, measured by X-ray diffraction, and the area ratio I_D/I_G for different carbon fibre sources (pyrolyzed wood, PAN and pitch-based) derived CF is presented in Figure 6b [35]. It can be seen that the maximum of I_D/I_G for Zickler *et al.*'s [35] work is located at $L_a \approx 2$ nm, consistent with Ferrari and Robertson's work [25]. The value of this maximum is different from the models used for our work because different Raman laser excitations were applied. The I_D/I_G value for the CNF/SiC/CNTs is found to be 1.31 ± 0.02; this sample could fit a model for either an $L_a > 2$ nm or $L_a < 2$ nm (see double-pointed arrow in Fig 5b). In addition, it is noted that the value of the I_D/I_G ratio for the CNF/SiC/CNTs sample is higher than for CNF2200 and CF2500 [19, 24]. This is because the latter two samples fit the model for a $L_a > 2$ nm *i.e.* equation 2. This higher value of I_D/I_G ratio for CNF/SiC/CNTs corresponds to a lower L_a, regardless of which model ($L_a > 2$ nm or $L_a < 2$ nm) is used. The Young's modulus for the CNF/SiC/CNTs is however higher than CNF2200 and CF2500 fibres. This suggests that the growth of CNTs improves the stiffness overall, even competitive with highly graphitized CNF. It is worthwhile noting that higher temperatures could still improve the modulus further. The Young's modulus of carbon materials also depends not only on the crystalline size, but additionally on the degree of preferred orientation and crystalline shape [36]. So, these properties could have an effect on the modulus values obtained.

It is thought that some load sharing might occur between SiC nanoparticles and carbon nanofibres. It is noted that no TO bands from the SiC nanoparticles are observed from the samples prepared for the Raman spectroscopic study. This is either because the CNTs have

fully covered the CNF/SiC surface, or that bands from the SiC overlap with those from PMMA. Therefore, load sharing between the SiC nanoparticles and the carbon nanofibres cannot be estimated using this approach. Nevertheless, using the electrospinning method to synthesise the CNF/SiC/CNTs composite fibres paves the way to produce high-performance SiC reinforced CF composite nanofibres.

4. Conclusions

CNF/SiC and CNF/SiC/CNTs composite fibres were fabricated from a cellulose precursor by electrospinning, and for the latter samples using a CVD technique. The polytype of the SiC nanoparticles in CA fibres was determined to be 3C-SiC by SAED using TEM. Raman spectroscopy shows that the CNF/SiC/CNTs samples have a higher crystallinity than the CNF/SiC samples when comparing the I_D/I_G ratios, and the FWHM of the D and G bands. An *in-situ* Raman spectroscopic study was used to determine the elastic modulus of the CNF/SiC/CNTs composite nanofibres. The 2D band exhibited a linear downshift with the application of tensile deformation. The elastic modulus of the CNF/SiC/CNTs was estimated to be 166 ± 28 GPa. The unique structure of these composite nanofibres, combined with their high stiffness, could enable them to be used to reinforce composite materials. Furthermore, the *in-situ* Raman deformation test has the potential to be used as a calibration for non-contact inspection of C/SiC based structures (*e.g.* brake pads) by converting the Raman shifts into stress.

Acknowledgements

We would like to thank the Chinese Scholarship Council and the University of Exeter for funding a PhD studentship (for QL). We also acknowledge the input of Professors O. Paris and

G. Zickler (Univ. Leoben) for their comments for the provision of data for Figure 6, and for assistance in interpreting Raman data for carbon.

5. References

[1] Chand S. Review Carbon fibers for composites. Journal of Materials Science. 2000;35(6):1303-13.

[2] Xu BS, Zhou SB, Hong CQ, Han JC, Zhang XH. Mechanical enhancement of lightweight ZrB2-modified carbon-bonded carbon fiber composites with self-grown carbon nanotubes. Carbon. 2016;102:487-93.

[3] Kaybal HB, Ulus H, Demir O, Sahin OS, Avci A. Effects of alumina nanoparticles on dynamic impact responses of carbon fiber reinforced epoxy matrix nanocomposites. Eng Sci Technol. 2018;21(3):399-407.

[4] Patnaik A, Satapathy A, Mahapatra SS, Dash RR. A Comparative Study on Different Ceramic Fillers Affecting Mechanical Properties of Glass—Polyester Composites. Journal of Reinforced Plastics and Composites. 2008;28(11):1305-18.

[5] Mehmet B, Mohamad A, Ahmet E. A comparative study on the tensile and impact properties of Kevlar, carbon, and S-glass/epoxy composites reinforced with SiC particles. Materials Research Express. 2018;5(2):025301.

[6] Xie W, Mirza Z, Mobus G, Zhang SW. Novel Synthesis and Characterization of High Quality Silicon Carbide Coatings on Carbon Fibers. J Am Ceram Soc. 2012;95(6):1878-82.

[7] Petroski K, Poges S, Monteleone C, Grady J, Bhatt R, Suib SL. Rapid Chemical Vapor Infiltration of Silicon Carbide Minicomposites at Atmospheric Pressure. ACS Appl Mater Interfaces. 2018;10(5):4986-92.

[8] Wang Y, Chen ZF, Yu SJ. Ablation behavior and mechanism analysis of C/SiC composites. J Mater Res Technol. 2016;5(2):170-82.

[9] Xie H, Fu K, Yang CP, Yao YG, Rao JC, Zhou YB, et al. Necklace-Like Silicon Carbide and Carbon Nanocomposites Formed by Steady Joule Heating. Small Methods. 2018;2(4):1700371.

[10] Xu ZL, Zhang B, Kim JK. Electrospun carbon nanofiber anodes containing monodispersed Si nanoparticles and graphene oxide with exceptional high rate capacities. Nano Energy. 2014;6:27-35.

[11] Li Q, Deng LB, Kim JK, Zhu YQQ, Holmes SM, Perez-Page M, et al. Growth of Carbon Nanotubes on Electrospun Cellulose Fibers for High Performance Supercapacitors. J Electrochem Soc. 2017;164(13):A3220-A8.

[12] Sharma SP, Lakkad SC. Effect of CNTs growth on carbon fibers on the tensile strength of CNTs grown carbon fiber-reinforced polymer matrix composites. Compos Part a-Appl S. 2011;42(1):8-15.

[13] Ye C, Ran G, Zhou W, Qu Y, Yan X, Cheng Q, et al. The Preparation and Microstructure of Nanocrystal 3C-SiC/ZrO(2) Bilayer Films. Nanomaterials-Basel. 2017;7(12):408.

[14] Zhang YF, Han XD, Zheng K, Zhang Z, Zhang XN, Fu JY, et al. Direct observation of super-plasticity of beta-SiC nanowires at low temperature. Adv Funct Mater. 2007;17(17):3435-40.

[15] Liu Y, Hou H, He X, Yang W. Mesporous 3C-SiC Hollow Fibers. Sci Rep. 2017;7(1):1893.

[16] Zhang K, Feldner A, Fischer S. FT Raman spectroscopic investigation of cellulose acetate. Cellulose. 2011;18(4):995-1003.

[17] Sánchez-Márquez J, Fuentes-Ramírez R, Cano-Rodríguez I, Gamiño-Arroyo Z, Rubio-Rosas E, Kenny J, et al. Membrane made of cellulose acetate with polyacrylic acid reinforced with carbon nanotubes and its applicability for chromium removal. International Journal of Polymer Science. 2015;2015.

[18] Ward Y, Young RJ, Shatwell RA. Application of Raman microscopy to the analysis of silicon carbide monofilaments. Journal of Materials Science. 2004;39(22):6781-90.

[19] Deng LB, Young RJ, Kinloch IA, Zhu YQ, Eichhorn SJ. Carbon nanofibres produced from electrospun cellulose nanofibres. Carbon. 2013;58:66-75.

[20] Parida B, Choi J, Lim G, Kim K, Kim K. Enhanced Visible Light Absorption by 3C-SiC Nanoparticles Embedded in Si Solar Cells by Plasma-Enhanced Chemical Vapor Deposition. J Nanomater. 2013;2013:10.

[21] Gadzira M, Gnesin G, Mykhaylyk O, Andreyev O. Synthesis and structural peculiarities of nonstoichiometric β-SiC. Diamond and Related Materials. 1998;7(10):1466-70.

[22] Bokobza L, Zhang J. Raman spectroscopic characterization of multiwall carbon nanotubes and of composites. Express Polym Lett. 2012;6(7):601-8.

[23] Dresselhaus MS, Jorio A, Souza Filho AG, Saito R. Defect characterization in graphene and carbon nanotubes using Raman spectroscopy. Philos T R Soc A. 2010;368(1932):5355-77.

[24] Kong K, Deng LB, Kinloch IA, Young RJ, Eichhorn SJ. Production of carbon fibres from a pyrolysed and graphitised liquid crystalline cellulose fibre precursor. Journal of Materials Science. 2012;47(14):5402-10.

[25] Ferrari AC, Robertson J. Interpretation of Raman spectra of disordered and amorphous carbon. Physical review B. 2000;61(20):14095.

[26] Matthews M, Pimenta M, Dresselhaus G, Dresselhaus M, Endo M. Origin of dispersive effects of the Raman D band in carbon materials. Physical Review B. 1999;59(10):R6585.

[27] Tuinstra F, Koenig JL. Raman Spectrum of Graphite. The Journal of Chemical Physics. 1970;53(3):1126-30.

[28] Pimenta MA, Dresselhaus G, Dresselhaus MS, Cancado LG, Jorio A, Saito R. Studying disorder in graphite-based systems by Raman spectroscopy. Phys Chem Chem Phys. 2007;9(11):1276-91.

[29] Ferrari AC. Raman spectroscopy of graphene and graphite: Disorder, electron-phonon coupling, doping and nonadiabatic effects. Solid State Commun. 2007;143(1-2):47-57.

[30] Frank O, Tsoukleri G, Riaz I, Papagelis K, Parthenios J, Ferrari AC, et al. Development of a universal stress sensor for graphene and carbon fibres. Nat Commun. 2011;2.

[31] Mohiuddin T, Lombardo A, Nair R, Bonetti A, Savini G, Jalil R, et al. Uniaxial strain in graphene by Raman spectroscopy: G peak splitting, Grüneisen parameters, and sample orientation. Physical Review B. 2009;79(20):205433.

[32] Cooper CA, Young RJ, Halsall M. Investigation into the deformation of carbon nanotubes and their composites through the use of Raman spectroscopy. Compos Part a-Appl S. 2001;32(3-4):401-11.

[33] Zhang QH, Liu JW, Sager R, Dai LM, Baur J. Hierarchical composites of carbon nanotubes on carbon fiber: influence of growth condition on fiber tensile properties. Compos Sci Technol. 2009;69(5):594-601.

[34] Lourie O, Wagner HD. Evaluation of Young's modulus of carbon nanotubes by micro-Raman spectroscopy. J Mater Res. 1998;13(9):2418-22.

[35] Zickler GA, Smarsly B, Gierlinger N, Peterlik H, Paris O. A reconsideration of the relationship between the crystallite size La of carbons determined by X-ray diffraction and Raman spectroscopy. Carbon. 2006;44(15):3239-46.

[36] Li D, Wang H, Wang X. Effect of microstructure on the modulus of PAN-based carbon fibers during high temperature treatment and hot stretching graphitization. Journal of materials science. 2007;42(12):4642-9.

Table 1. I_D/I_G and FWHM of D and G bands for CNF/SiC and CNF/SiC/CNTs.

		FWHM (cm^{-1})	
Sample	I_D/I_G	D band	G band
CNF/SiC	1.19 ± 0.02	250.8 ± 3.0	99.4 ± 2.0
CNF/SiC/CNTs	1.31 ± 0.02	149.1 ± 1.3	69.3 ± 1.1

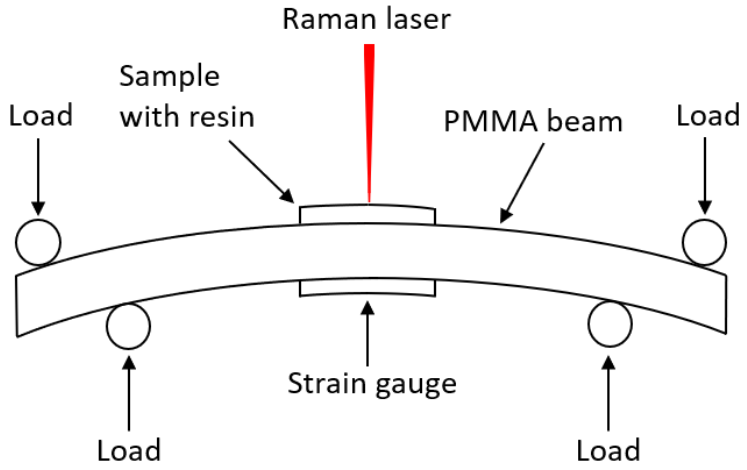

Figure 1 A typical schematic of *in-situ* Raman spectroscopy and deformation tests.

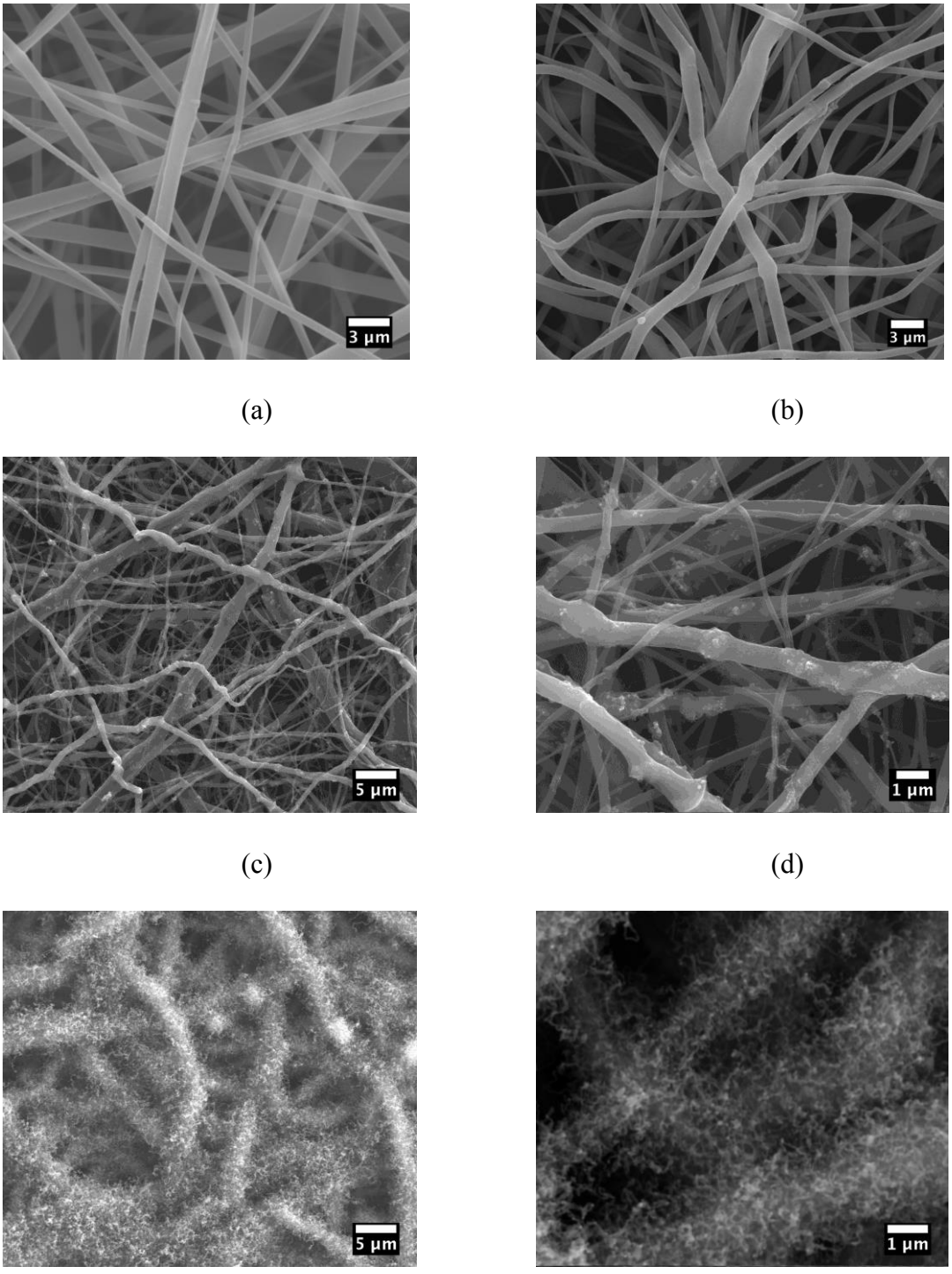

Figure 2 Typical SEM images of (a) as-spun CA fibre/SiC, (b) regenerated cellulose fibre/SiC and (c) CNF/SiC; (d) an enlarged image of CNF/SiC; (e) CNF/SiC/CNTs fibres and (f) an enlarged image of the CNF/SiC/CNTs fibres.

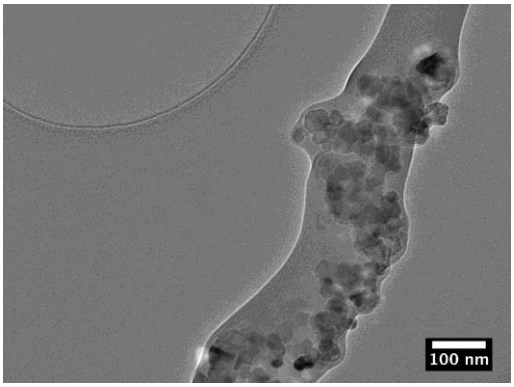

(a)

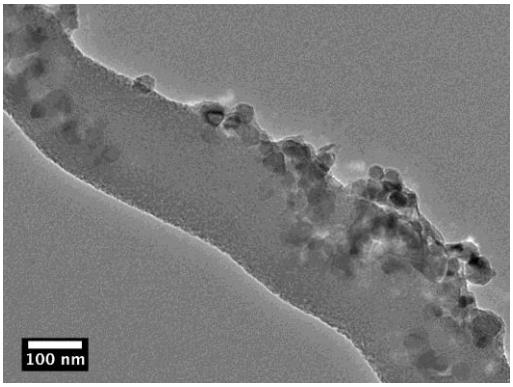

(b)

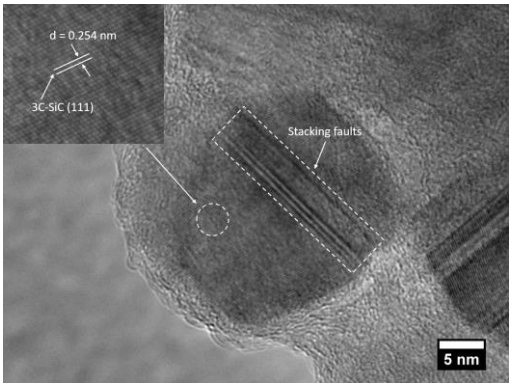

(c)

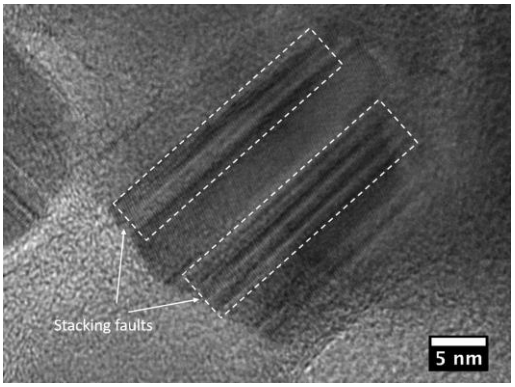

(d)

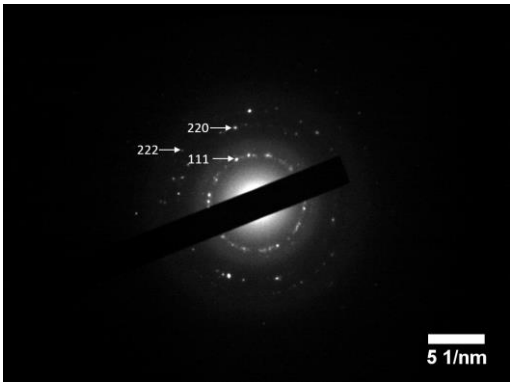

(e)

Figure 3 A typical TEM image of (a) as-spun CA with SiC nanoparticles and (b) CNF/SiC; (c) A typical SiC nanoparticle encapsulated in the CA with a 0.25 nm d-spacing of the 3C-SiC (111) planes (inset) – stacking faults also indicated; (d) A typical SiC nanoparticle with stacking faults (labeled with dashed rectangles); (e) An indexed SAED pattern for the SiC nanoparticle in (c).

(a)

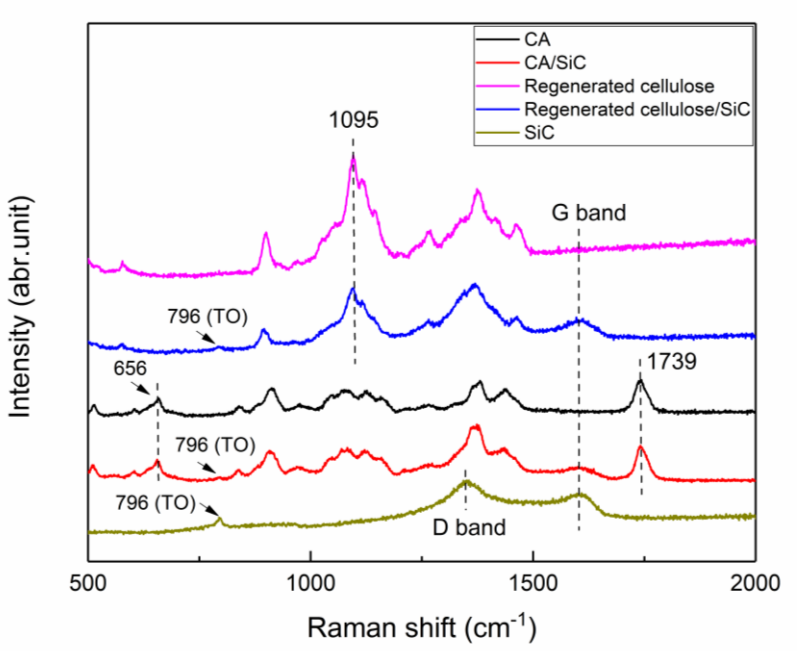

(b)

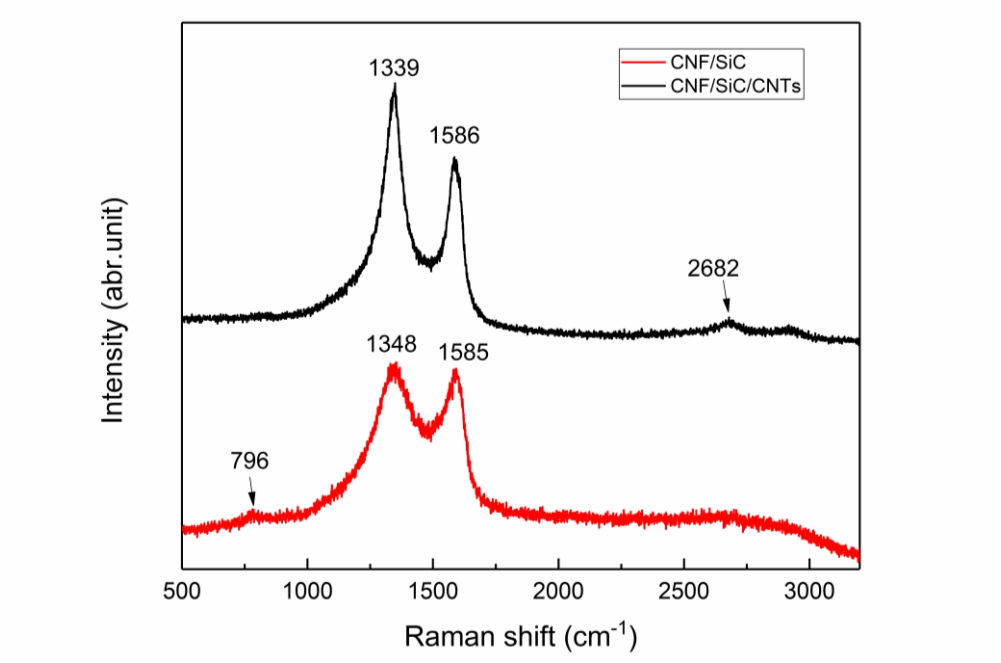

Figure 4 Typical Raman spectra of (a) SiC nanoparticles, CA, CA/SiC, regenerated cellulose, and regenerated cellulose/SiC fibres and (b) CNF/SiC, and CNF/SiC/CNTs nanofibres indicating the presence of bands located at ~796, 1339, 1348, 1585, 1586 and 2682 cm^{-1}.

(a)

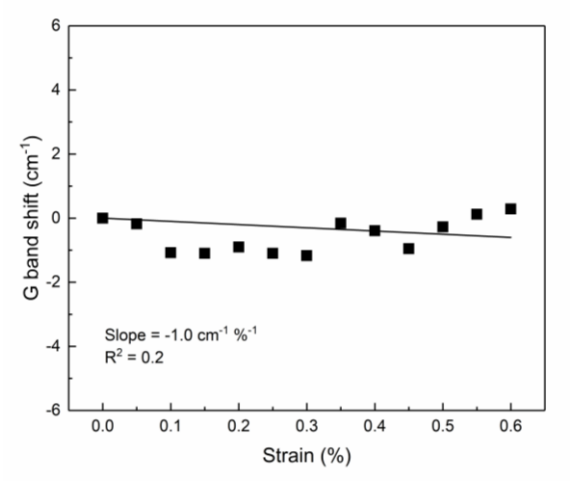

(b)

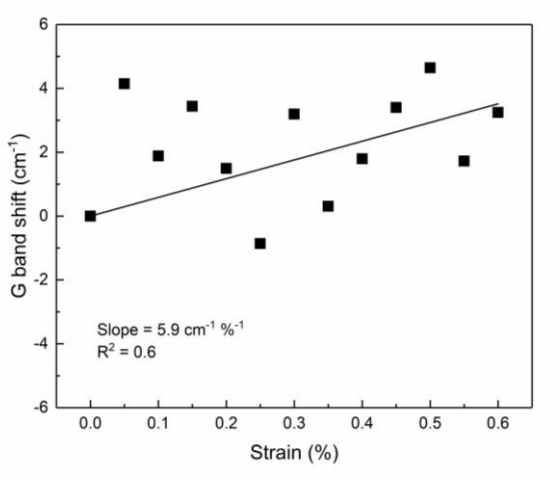

(c)

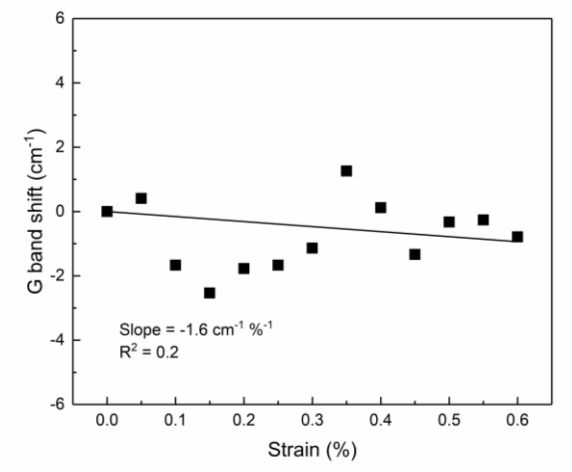

Figure 5 Typical plots of Raman G band shift versus strain for (a) CNF, (b) CNF/SiC, and (c) CNF/SiC/CNTs samples, with linear regressions to the data (black line).

(a)

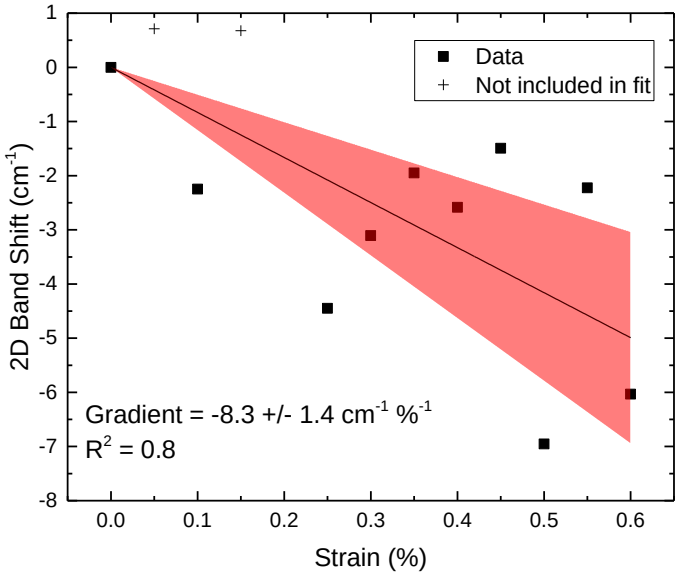

(b)

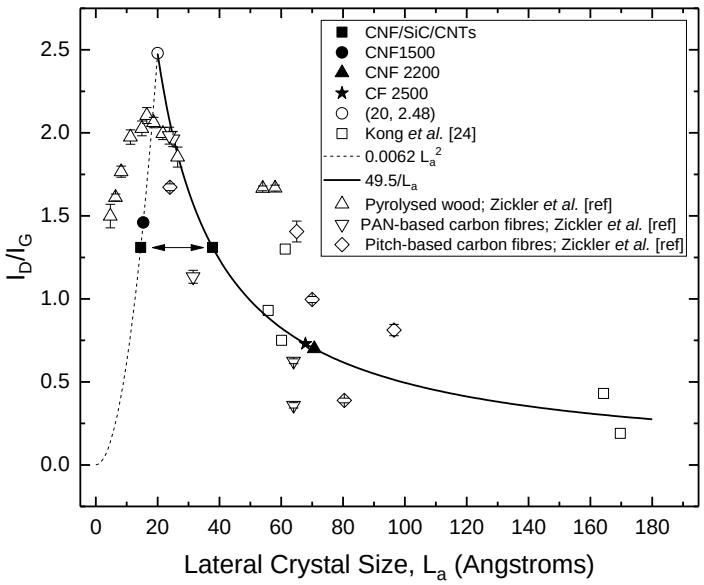

Figure 6 (a)Typical Raman shift of the 2D band with tensile deformation applied to the CNF/SiC/CNTs sample in 4-point bending. Solid line is a linear regression to the data. Shaded region are the 95% confidence bands. Data labelled + are not included in the fit; (b) L_a *versus* I_D/I_G for CNF/SiC/CNTs compared to data from published work [19, 24, 35]. The solid line represents the equation $I_D/I_G = 49.5/L_a$, and the dashed line is the relationship I_D/I_G

= 0.0062 L_a^2. A double pointed arrow refers to the alternative positions for the I_D/I_G ration for CNF/SiC/CNTs.